ISSN 1063-7834, Physics of the Solid State, 2012, Vol. 54, No. 4, pp. 790–797. © Pleiades Publishing, Ltd., 2012.
Original Russian Text © S.V. Razorenov, G.I. Kanel', G.V. Garkushin, O.N. Ignatova, 2012, published in Fizika Tverdogo Tela, 2012, Vol. 54, No. 4, pp. 742–749.

MECHANICAL PROPERTIES, PHYSICS OF STRENGTH, AND PLASTICITY

Resistance to Dynamic Deformation and Fracture of Tantalum with Different Grain and Defect Structures

S. V. Razorenov[a], G. I. Kanel'[b], G. V. Garkushin[a, *], and O. N. Ignatova[c]

[a] *Institute of Problems of Chemical Physics, Russian Academy of Sciences, av. Akademika Semenova 1, Chernogolovka, Moscow region, 142432 Russia*

* *e-mail: garkushin@ficp.ac.ru*

[b] *Joint Institute for High Temperatures, Russian Academy of Sciences, Izhorskaya st. 13-2, Moscow, 125412 Russia*

[c] *Russian Federal Nuclear Center—The All-Russia Research Institute of Experimental Physics, av. Mira 37, Sarov, Nizhni Novgorod region, 607188 Russia*

Received September 19, 2011

Abstract—This paper presents the results of measurements of the strength properties of technically pure tantalum under shock wave loading. It has been found that a decrease in the grain size under severe plastic deformation leads to an increase in the hardness of the material by approximately 25%, but the experimentally measured values of the dynamic yield stress for the fine-grained material prove to be less than those of the initial coarse-grained specimens. This effect has been explained by a higher rate of stress relaxation in the fine-grained material. The hardening of tantalum under shock wave loading at a pressure in the range 40–100 GPa leads to a further increase in the rate of stress relaxation, a decrease in the dynamic yield stress, and the disappearance of the difference between its values for the coarse-grained and fine-grained materials. The spall strength of tantalum increases by approximately 5% with a decrease in the grain size and remains unchanged after the shock wave loading. The maximum fracture stresses are observed in tantalum single crystals.

DOI: 10.1134/S1063783412040233

1. INTRODUCTION

It is known that plastic deformation results in a hardening of metals and alloys due to an accumulation of deformation defects [1] and, in the case of severe deformations, due to a decrease in grain size [2–4]. However, the data available in the literature on the influence of these factors on the flow stress and strength of materials under high strain rate loading [5–8] are very scarce and contradictory. While the hardness, yield stress, and tensile strength, which are measured under low strain rate loading, increase after severe plastic deformation or shock wave loading of the material, changes in the resistance to high strain rate loading and fracture can be not observed or even have the opposite sign. At the same time, the development of models describing the high strain rate loading and fracture and the construction of the corresponding basic relationships, which are necessary for calculations of intensive pulsed loading, are impossible without a clear understanding of the contributions from different structural factors to these processes over a wide range of loading durations. In order to fill this gap, in the present work we have performed systematic investigations of the behavior of tantalum with different grain sizes and different degrees of imperfection under shock wave loading.

Interest expressed by researchers in the spall strength of tantalum is associated with its practical application in constructions operating under intensive pulsed loading (for example, under conditions of an explosion and a high-velocity impact). Tantalum has a body-centered cubic structure of the crystal lattice, a density of 16.6 g/cm^3, and a melting point of 3287 K and exhibits a combination of high hardness with high plasticity. The elastoplastic properties and spall fracture of tantalum under shock wave loading have been investigated in a rather large number of works [9–22], which, however, have remained unclear the mechanism of the influence of structural factors on these processes. The dynamic elastic limit for tantalum, according to different data, varies in the range from 1.5 to 4.5 GPa, and the spall strength lies in the range from 5 to 10 GPa. The metallographic analysis of tantalum specimens after shock wave loading [21] has demonstrated that, beginning with the shock compression pressure in the range between 7 and 14 GPa, in the material there appear twins whose volume fraction increases with increasing pressure to 45 GPa. The twinning of single crystals strongly depends on the direction of shock loading with respect to the crystallographic axes of tantalum [22]. The spall strength slightly increases with a decrease in the grain size and can substantially vary even within a single specimen. In this case, the fracture nucleation occurs at grain

Table 1. Hardness of tantalum in different structural states

Specimen type	Hardness, HRB
Initial coarse-grained (CG)	76–79
Ultrafine-grained (UFG)	103–104
Single-crystal	68
Coarse-grained after the shock compression (~40 GPa)	103
Coarse-grained after the shock compression (~100 GPa)	97–99
Ultrafine-grained grained after the shock compression (~40 GPa)	104–105
Ultrafine-grained grained after the shock compression (~100 GPa)	103–105

boundaries; during the growth, the initial intergrain microcracks transform into round pores [10, 11, 13], which correlates with the high plasticity of the material.

2. MATERIALS AND EXPERIMENTAL TECHNIQUE

The initial material (TVCh grade) contained 99.9% tantalum and had an average grain size of approximately 50–60 μm. In order to obtain an ultrafine-grained structure, the coarse-grained tantalum specimens were subjected to a repeated round forging in different high-temperature regimes [3]. After severe plastic deformation, the average grain size was reduced to ~0.5–0.6 μm; the grain structure after this treatment was fairly homogeneous.

The degree of imperfection of the coarse-grained and fine-grained materials was varied by means of the shock wave loading. The electron microscopic analysis revealed that the coarse-grained material subjected to shock wave treatment undergoes intensive twinning, so that the volume fraction of twins varied in the range 10–20% depending on the shock compression pressure. Since the high strain rate loading in a shock wave was accompanied by an increase in temperature, the residual density of twins after the loading at a pressure of 100 GPa due to the annealing appeared to be somewhat lower than that after shock wave treatment at a pressure of 40–60 GPa. The electron microscopic analysis of the fine-grained material subjected to shock wave treatment revealed that the specimen contained only a few twins with a thickness of 0.2–0.3 μm. The dislocation density in coarse-grained tantalum after the shock wave loading increased from 0.5×10^{10} to 2.0×10^{10} cm^{-2} with an increase in the shock compression pressure to 100 GPa.

Table 1 presents the obtained data on the hardness of all the types of tantalum specimens examined in the present work. It should be noted that, after the preliminary shock compression, the hardness increases only in the initial coarse-grained specimens and remains almost unchanged in the ultrafine-grained material.

The experiments were carried out using specimens with thicknesses of ~0.5–0.6 and ~2.0 mm, which were cut from blanks by the electric spark method. The transverse dimension of the specimens was varied in the range 25–30 mm. The shock wave loading of the specimens was performed by an impact with an aluminum plate having a thickness of 0.12 mm (for the specimens with a thickness of 0.6 mm) or 0.4 mm. For this ratio between the thicknesses of the specimen and the impact plate, the profile of the compression pulse by the time of its appearance on the free surface became approximately triangular in shape, which decreased the error in the determination of the spall strength of the material [23]. The experiments carried out with different thicknesses of the specimens made it possible to change the rate of tensile strain of tantalum in the unloading wave before the fracture by a factor of approximately 5. Throwing of the impact plates with a velocity of ~1250 ± 50 m/s was performed using an explosive device [24]. For this impact velocity, the pressure of shock compression of the tantalum specimens was equal to ~14 GPa, and the strain in the direction of uniaxial compression was $\varepsilon_x = 1 - V/V_0 = 0.075$. In our experiments, the free-surface velocity profiles were recorded using a laser Doppler velocimeter VISAR [24, 25].

3. RESULTS OF MEASUREMENTS

The results of measurements of the free-surface velocity profiles $u_{fs}(t)$ of the initial coarse-grained (CG) and ultrafine-grained (UFG) tantalum specimens are compared in Fig. 1.

The wave profiles demonstrate that an elastic precursor, a plastic shock wave, and a part of the subsequent rarefaction wave appear on the surface. The time of increase in the parameters in the plastic shock wave is determined by the viscosity of the material or by the time of stress relaxation. For the chosen ratio between thicknesses of the impact plate and the specimen, the loading conditions in the vicinity of the free rear surface of the specimen correspond to the onset of attenuation of the shock wave under the action of the overtaking rarefaction wave, and the unloading immediately follows the compression wave and decreases the velocity of the particles of the material. After the reflection of the compression pulse from the free sur-

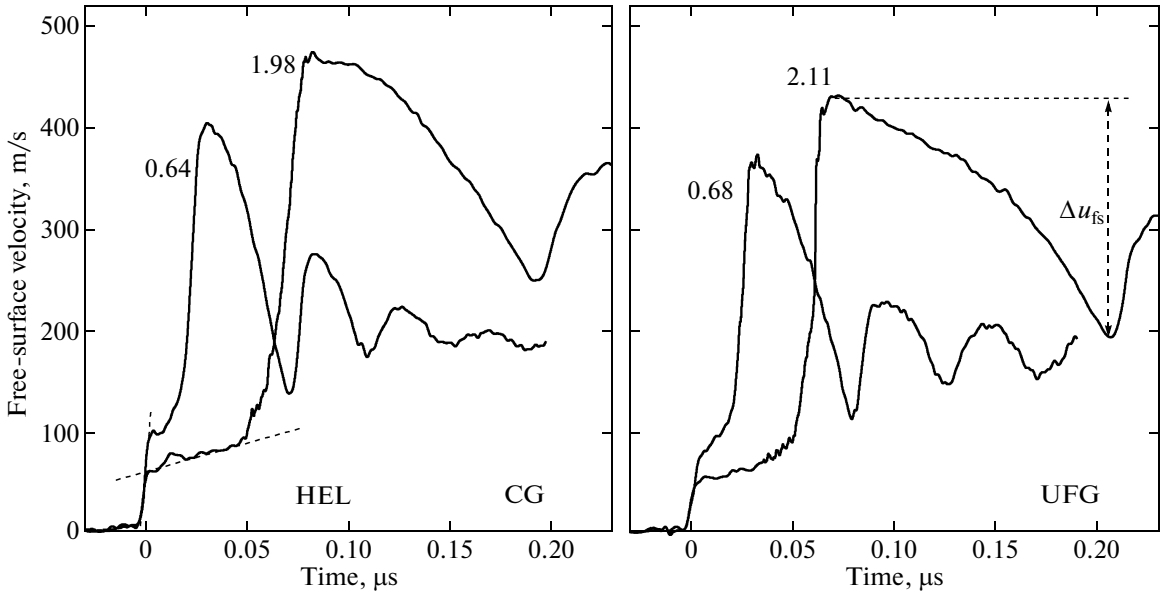

Fig. 1. Results of measurements of the free-surface velocity profiles of the initial coarse-grained (CG) and ultrafine-grained (UFG) tantalum specimens. Numbers near the velocity profiles are the thicknesses of specimens (in millimeters).

face, the tensile stresses are generated inside the specimen, which, in turn, initiates its fracture, i.e., a spall. This is accompanied by the relaxation of tensile stresses and the formation of a compression wave (spall pulse), which comes to the surface of the specimen and causes the second increase of its velocity. A further decay of oscillations of the velocity is related to the reverberation of the spall pulse in the "spall plate" detached from the specimen.

The compressive stress behind the front of the elastic precursor, i.e., the dynamic elastic limit σ_{HEL}, is calculated from the measured free-surface velocity u_{HEL} according to the expression $\sigma_{HEL} = \rho_0 c_l u_{HEL}/2$. The corresponding values of the yield stress are given by the formula $Y = (3/2)\sigma_{HEL}(1 - c_b^2/c_l^2) = 2\sigma_{HEL}C/E'$, where $G = (3/4)\rho_0(c_l^2 - c_b^2)$ is the shear modulus; $E' = \rho_0 c_l^2$ is the modulus of elongation (Young's modulus); c_l and c_b are the longitudinal and bulk velocities of sound, respectively; and ρ_0 is the density of the material. In the processing of the wave profiles containing small irregular oscillations and other distortions, the free-surface velocity u_{HEL} is determined by the extrapolation to the front of the elastic precursor of the linear approximation of a part of the wave profile behind the front of the precursor, as is shown in Fig. 1.

The free-surface velocity decrement Δu_{fs}, when the free-surface velocity decreases from the maximum to the value before the front of the spall pulse (Fig. 1), is proportional to the fracture stress, i.e., the spall strength of the material σ_{sp} under the given loading conditions. In the linear (acoustic) approximation, we can write

$$\sigma_{sp} = \frac{1}{2}\rho_0 c_b(\Delta u_{fs} + \delta u),$$

where δu is the correction for distortion of the wave profile due to the differences between the velocities of the spall pulse front and the velocity of the plastic part of the incident unloading wave before this front [23]. The thickness of the spall plate h is determined by the period Δt of oscillations of the free-surface velocity after the spall according to the expression $h = c_l\Delta t/2$.

Table 2 presents the results of measurements of the resistance to high strain rate loading and fracture of tantalum specimens with different structures under shock wave loading. The designations used in this table are as follows: h_{sam} is the thickness of the specimen, h_{imp} is the thickness of the impact plate, σ_{HEL} is the dynamic elastic limit, Y is the tensile stress behind the front of the elastic precursor, σ_{sp} is the spall strength, h_{sp} is the thickness of the spall plate; and $\dot{V}/V_0$ is the rate of expansion of the material before the front of the spall pulse.

4. FLOW STRESS OF TANTALUM

The performed measurements have demonstrated a significant decay of the elastic precursors during the propagation in both the initial coarse-grained and ultrafine-grained tantalum materials. The elastic precursor decay is caused by the relaxation of deviator stresses due to the development of plastic deformation

Table 2. Results of measurements of the strength properties of tantalum under shock wave loading

Specimen no.	h_{sam}, mm	h_{imp}, mm	σ_{HEL}, GPa	Y, GPa	σ_{sp}, GPa	h_{sp}, mm	$\dot{V}/V_0$, 10^5 s^{-1}
Initial coarse-grained tantalum (CG)							
20	1.97	0.4	2.12	1.02	6.7	0.21	3.1
21	0.64	0.11	3.24	1.56	8.1	0.08	13
Ultrafine-grained tantalum (UFG)							
9	2.14	0.41	2.05	0.99	7.1	0.26	4.5
10	2.11	0.41	1.83	0.88	7.6	0.26	4.8
11	0.68	0.12	2.66	1.28	7.9	0.09	12
12	0.54	0.12	2.2	1.06	8.4	0.07	19
Tantalum CG after the shock compression 40 GPa							
18	1.97	0.41	1.6	0.77	6.5	0.24	3.7
19	0.56	0.11	1.97	0.95	7.6	0.08	12
Tantalum UFG after the shock compression 40 GPa							
22	1.97	0.41	1.7	0.82	7.5	0.25	4.7
23	0.59	0.11	2.0	0.96	7.9	0.09	14
Tantalum after the shock compression 100 GPa							
25(CG)	1.92	0.41	1.5	0.72	6.9	0.29	3
24(UFG)	1.97	0.41	–		7.4	0.25	3.9
Tantalum CG after the shock compression at a velocity of 4.1 km/s							
27	1.98	0.38			7.3	0.084	8.5
Single-crystal tantyalum							
13	2.02	0.41	2.2	1.06	9.4	0.3	3.9
15	1.98	0.41	1.7	0.82	10.4	0.29	5
16	0.46	0.12	–		9.6	0.09	6

immediately behind the elastic wave and is related to the plastic strain rate $\dot{\gamma}$ by the expression [26]

$$\left.\frac{d\sigma}{dh}\right|_{HEL} = -\frac{4}{3}\frac{G\dot{\gamma}_p}{c_l},$$

where h is the distance traversed by the elastic wave. The data presented in Fig. 1 indicate that, in the coarse-grained material, the dynamic elastic limit σ_{HEL} decreases from 3.24 GPa at a distance of 0.64 mm to 2.12 GPa at a distance of 1.98 mm. In the ultrafine-grained tantalum, the value of σ_{HEL} varies in the range from 2.66 GPa at a distance of 0.68 mm to 1.83 GPa at a distance of 2.11 mm. After the severe plastic deformation, the hardness of tantalum increases by approximately 25% (Table 1), whereas the dynamic elastic limit σ_{HEL} becomes even slightly lower than that for the initial coarse-grained material. This difference is particularly evident in the experiments on the specimens with a thickness of ~0.65 mm.

The time of increase in the parameters in the plastic shock wave for the ultrafine-grained specimens is noticeably shorter. This indicates a higher rate of plastic deformation and, probably, a lower characteristic viscosity $\tau/\dot{\varepsilon}$ of the material. A decrease in the viscosity after the severe plastic deformation was previously observed for other metals [7]. The maximum compressive strain rate in the shock wave $\dot{\varepsilon}_{max} = \dot{u}_{fs,\,max}/2U_S$ in accordance with the measured values of the maximum acceleration of the free surface $\dot{u}_{fs,\,max}$, which are equal to 26 (km/s) μs^{-1} for coarse-grained tantalum and 47 (km/s) μs^{-1} for ultrafine-grained tantalum at a plastic shock wave velocity of 3.7 km/s, is estimated to be 3.5×10^6 s^{-1} for coarse-grained tantalum and 6.4×10^6 s^{-1} for ultrafine-grained tantalum.

Probably, the observed difference in the manifestations of the effects of comminution of the grain structure under conventional conditions of low strain rate loading and high rate shock wave compression is explained by different rates of stress relaxation in the coarse-grained and ultrafine-grained tantalum materials and by different rates of the elastic precursor decay, as is schematically shown in Fig. 2. At large distances, the stresses behind the elastic precursors should approach the values corresponding to the quasi-static yield stresses. In other words, the dynamic elastic limit σ_{HEL} measured on specimens with a large thickness should be higher for the ultrafine-grained tantalum material as compared to that for the coarse-grained tantalum material. However, if the characteristic viscosity of the harder ultrafine-grained tantalum

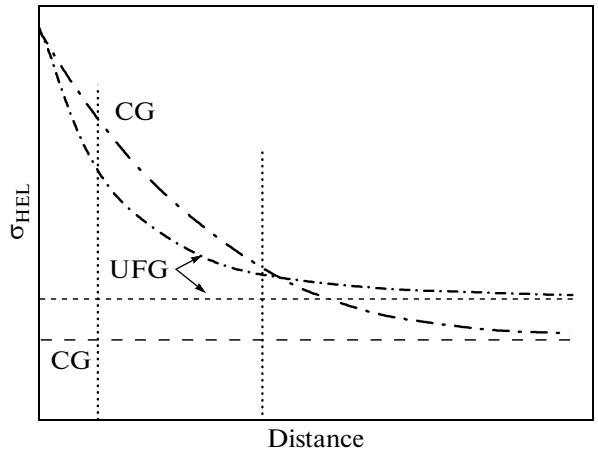

Fig. 2. Estimated difference in the rates of decay of the elastic precursors in the coarse-grained (CG) and ultrafine-grained (UFG) tantalum specimens. Vertical lines indicate the thicknesses of the specimens in the performed measurements.

material is lower than the viscosity of the coarse-grained tantalum material, the elastic precursor decay in the ultrafine-grained tantalum occurs more rapidly than in the coarse-grained tantalum. As a result, for the specimens with a small thickness, there can occur a situation corresponding to the region between vertical lines in Fig. 2, where the harder ultrafine-grained tantalum demonstrates lower values of the dynamic elastic limit than the coarse-grained material.

Figure 3 presents the results of experiments with specimens of the initial coarse-grained and ultrafine-grained tantalum materials subjected to shock wave loading at a shock compression pressure of 40 GPa. All the results of measurements of the dynamic elastic limit as a function of the thickness of the specimens are summarized in Fig. 4.

The shock wave treatment leads both to a decrease in the values of the dynamic elastic limit of the coarse-grained and ultrafine-grained tantalum materials and to a decrease in the difference between these values. The rates of elastic precursor decay also decrease in the studied range of specimen thicknesses. It should be noted that the rates of compression in the plastic shock wave after the shock wave treatment increase to $(0.95–1.10) \times 10^7$ s^{-1} and differ only slightly for the two types of material. An increase in the pressure of preliminary shock compression to 100 GPa result in a dispersion of the elastic precursor front without a substantial change in the other measured characteristics.

5. SPALL STRENGTH OF TANTALUM

The measurements of the spall strength of tantalum materials with different grain structures were supplemented by the experiments with single-crystal tantalum. The orientation of tantalum single crystals with respect to the directions of propagation of shock wave loading was not determined. In similar experiments performed earlier with molybdenum [27], it was found that the influence of the orientation on the resistance to spall fracture is not very significant. Figure 5 shows

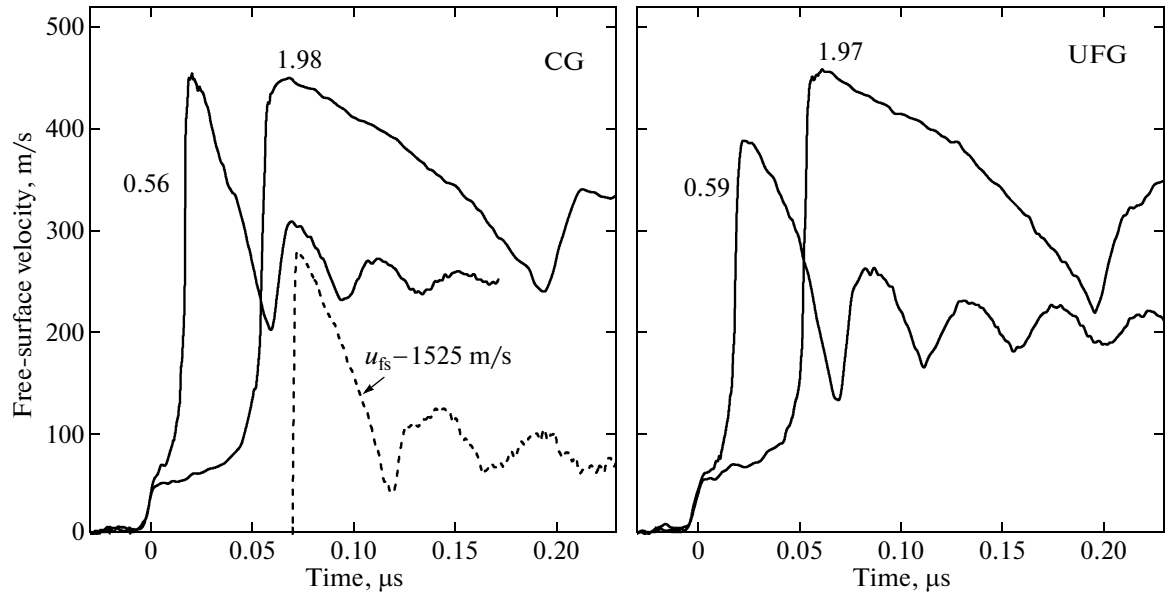

Fig. 3. Results of measurements of the free-surface velocity profiles of the initial coarse-grained (CG) and ultrafine-grained (UFG) tantalum specimens preliminarily subjected to shock compression at a pressure of 40 GPa. Numbers near the velocity profiles are the thicknesses of specimens (in millimeters). The dashed line shows the free-surface velocity profile u_{fs} measured for the coarse-grained tantalum specimen under a shock with a velocity of 4.1 km/s. The velocity profile is shifted by 1525 m/s (a multiple of the VISAR constant) toward lower velocities.

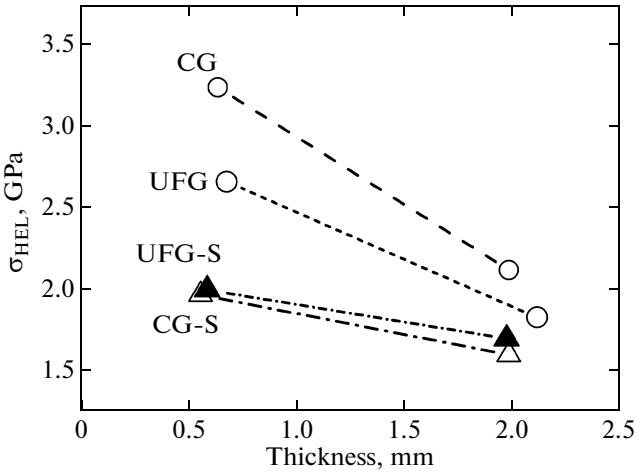

Fig. 4. Elastic precursor decay in tantalum specimens in the initial coarse-grained (CG) and ultrafine-grained (UFG) states and after shock wave loading at a shock compression pressure of 40 GPa (CG-S and UFG-S, respectively).

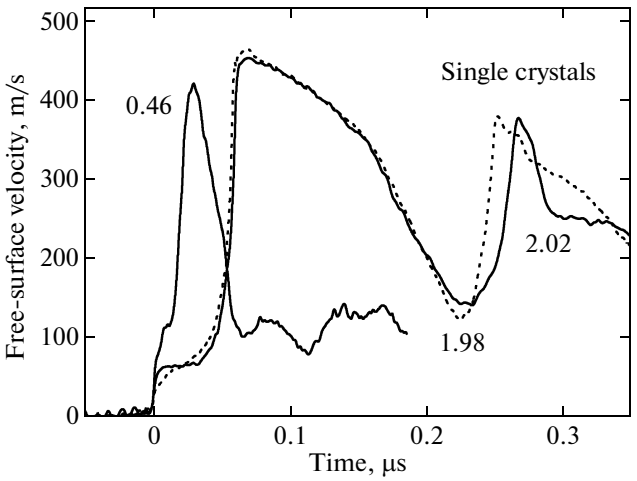

Fig. 5. Results of measurements of the free-surface velocity profiles of the single-crystal tantalum specimens. Numbers near the velocity profiles are the thicknesses of specimens (in millimeters).

the free-surface velocity profiles obtained in the experiments carried out for single-crystal tantalum specimens. A direct comparison of the data presented in Figs. 1, 3, and 5 has demonstrated that the tantalum single crystals free from structural defects exhibit a significantly higher resistance to spall fracture than polycrystalline tantalum. Furthermore, as judged from the shape of the free-surface velocity profiles directly in front of the spall pulse, the strength recourse of the material in these experiments has not been completely realized and, probably, higher values of the spall strength could be observed at a higher peak pressure of shock compression.

Taking into account that, according to the data available in the literature, there is a dependence of the resistance to spall fracture on the peak pressure in the incident loading pulse, we additionally performed measurements of the spall strength of the initial tantalum specimen with a thickness of 1.98 mm under loading by an impact with a 0.38-mm-thick aluminum plate at a velocity of 4.1 km/s. For this impact velocity, the pressure of shock compression of tantalum was equal to ~70 GPa against the pressure equal to ~14 GPa in the main series of experiments. The free-surface velocity profile measured in this case is presented in Fig. 3.

The high-rate fracture with a spall represents a kinetic process of generation, growth, and coalescence of a great number of discontinuities [28], and the observed values of the resistance to fracture are the result of competition of the growth of tensile stresses in the process of wave interactions and their relaxation due to the emergence and growth of discontinuities in the material. For this reason, the measured resistance to fracture at the spall increases with an increase in the strain rate.

The results of measurements of the spall strength of tantalum are summarized in Table 2 and Fig. 6, where they are represented as the dependence on the rate of expansion of the material in the rarefaction wave, which is defined as

$$\frac{\dot{V}}{V_0} = -\frac{\dot{u}_{\text{fsr}}}{2c_b},$$

where $\dot{u}_{\text{fsr}}$ is the measured rate of decrease in the free-surface velocity of the studied specimen in the unloading part of the shock compression pulse. In [24, 27, 29], it was shown that the initial rate of increase in the relative volume of discontinuities at the spall is equal to the expansion rate thus calculated for the material in the unloading wave, to within a constant factor of ~(2–4).

It can be seen from the presented results that a decrease in the grain size leads to an increase in the spall strength of tantalum by approximately 5%. The effect is somewhat more pronounced at a longer duration of the shock compression pulse. This result is not as obvious as one might expect, based on information about the behavior of materials under normal conditions. In polycrystalline tantalum, incipient cracks or pores in the spall are formed at the grain boundaries. For this reason, single crystals are characterized by a higher resistance to spall fracture as compared to polycrystalline tantalum. Most likely, the decrease in the size of grains under severe plastic deformation is also accompanied by the reduction of inclusions and other potential fracture sources concentrated at the grain boundaries.

The preliminary treatment of tantalum under shock compression almost did not affect the fracture stresses at the spall or slightly decreased the spall

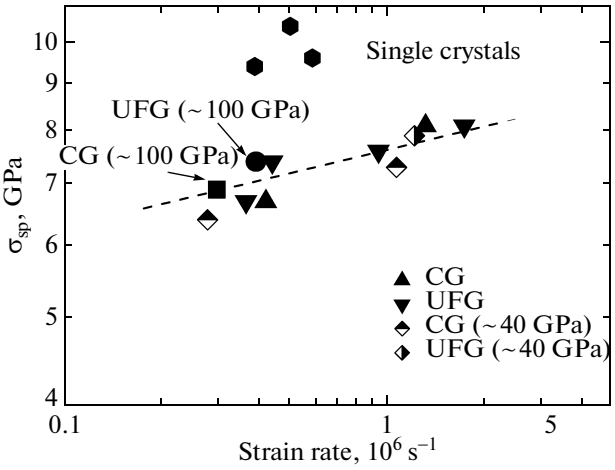

Fig. 6. Results of measurements of the dynamic strength of tantalum in different structural states.

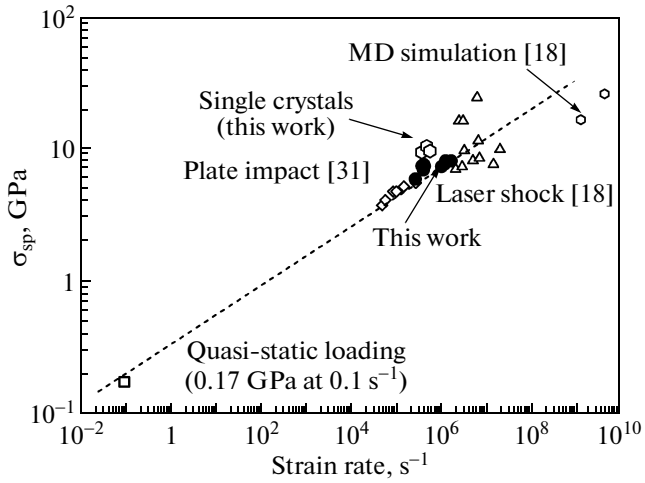

Fig. 7. Dependence of the spall strength of tantalum on the strain rate according to different authors.

strength σ_{sp}. A nearly fivefold increase in the shock compression pressure in the measurement of the spall strength produced a similar effect. Probably, twins and dislocations generated by a shock wave can make only a small contribution to the fracture nucleation at least in the studied range of stain rates. As regards the reports on the increase in the spall strength with an increase in the peak pressure in the incident loading pulse, this effect most likely is apparent and stems from the errors in the performance of the measurements. A detailed discussion of this aspect of the problem can be found in [30].

Figure 7 presents the results obtained in this work together with the results obtained from measurements of the spall strength of tantalum by the French authors Cuq-Lelandias et al. [18] and Roy [31]. It can be seen from this figure that, in the case where the spall is initiated by a laser pulse, the spread of the data on the spall strength at the same strain rate can reach 50% and more. For a plane collision of the plates, when the strain rate before the fracture varies in the range from 5×10^4 to 5×10^6 s^{-1}, such a strong spread of the measured spall strength is not observed even for tantalum with different grain structures. It seems likely that the instability of data on the spall strength appears when the thickness of the spall becomes smaller than the grain size. On the whole, our results are in good agreement with the data obtained by other authors, and the total dependence is reasonably extrapolated to the value of the strength of tantalum under low strain rate loading.

6. CONCLUSIONS

We have obtained new data on the strength properties of technically pure tantalum (TVCh grade) under submicrosecond shock wave loading. The most interesting and unexpected result is that a decrease in the grain size from 60.0 to 0.5 μm under severe plastic deformation, which leads to an increase in the hardness of the material by approximately 25%, has the opposite effect on the dynamic yield stress. This effect has been explained by a higher rate of stress relaxation in the fine-grained material. An accelerated relaxation of stresses in the fine-grained material also manifests itself in a higher rate of compression in a plastic shock wave. Apparently, the grain boundaries under these conditions are dislocation nucleation sites that ensure higher strain rate loading of the fine-grained material.

The hardening of tantalum under shock wave loading at a pressure in the range 40–100 GPa leads to an increase in the rate of stress relaxation, a decrease in the dynamic yield stress, and the disappearance of the difference between its values for the coarse-grained and fine-grained materials.

The spall strength of tantalum increases by approximately 5% with a decrease in the grain size and remains unchanged after the shock wave loading. A fivefold-increase in the pressure of shock wave compression preceding the spall also does not lead to a noticeable change in the fracture stress. Apparently, twins and dislocations generated by the shock wave can make only a small contribution to the fracture nucleation at least in the studied range of strain rates. The measured values of the spall strength are in agreement with the data available in the literature. The maximum fracture stresses are observed in tantalum single crystals.

ACKNOWLEDGMENTS

We would like to thank V.A. Salishchev for the assistance in the preparation of ultrafine-grained tantalum specimens and performance of their metallographic investigations and L.G. Ermolov for the assis-

tance in the preparation and performance of explosive experiments.

This study was supported by the Russian Foundation for Basic Research (project no. 08-02-00087a) and the Nuclear Energy State Corporation "ROSATOM" (state contract no. N.4e.45.03.09.1073).

REFERENCES

1. *Shock Waves and High-Strain-Rate Phenomena in Metals*, Ed. by M. A. Meyers and L. E. Murr (Plenum, New York, 1981; Metallurgiya, Moscow, 1984).
2. R. Z. Valiev and I. V. Aleksandrov, *Nanostructured Materials Produced by Severe Plastic Deformation* (Logos, Moscow, 2000) [in Russian].
3. R. Z. Valiev and I. V. Aleksandrov, *Bulk Nanostructured Metal Materials: Production, Structure and Properties* (Akademkniga, Moscow, 2007) [in Russia].
4. Yu. R. Kolobov and R. Z. Valiev, *Grain Boundary Diffusion and Properties of Nanostructured Materials* (Nauka, Novosibirsk, 2001; Cambridge International Science, Cambridge, 2007).
5. G. I. Kanel', S. V. Razorenov, and V. E. Fortov, Izv. Akad. Nauk, Mekh. Tverd. Tela, No. 4, 86 (2005).
6. S. V. Razorenov, A. S. Savinykh, E. B. Zaretsky, G. I. Kanel, and Yu. R. Kolobov, Phys. Solid State **47** (4), 663 (2005).
7. G. V. Garkushin, O. N. Ignatova, G. I. Kanel', L. Meier, and S. V. Razorenov, Izv. Akad. Nauk, Mekh. Tverd. Tela, No. 4, 155 (2010).
8. S. V. Razorenov, G. V. Garkushin, G. I. Kanel', O. A. Kashin, and I. V. Ratochka, Phys. Solid State **53** (4), 824 (2011).
9. P. P. Gillis, K. G. Hoge, and R. J. Wasley, J. Appl. Phys. **42**, 2145 (1971).
10. T. A. Manson, B. L. Henrie, and K. A. Thomas, in *Proceedings of the 14th APS Topical Conference on Shock Compression of Condensed Matter, Baltimore, Maryland, United States, July 31–August 5, 2005*, Ed. by M. D. Furnish, M. L. Elert, T. P. Russell, and C. T. White (AIP Conf. Proc. (2006)), p. 638.
11. D. L. Tonks, B. L. Henrie, C. P. Trujillo, D. Holtkamp, and W. R. Thissell, in *Proceedings of the 14th APS Topical Conference on Shock Compression of Condensed Matter, Baltimore, Maryland, United States, July 31–August 5, 2005*, Ed. by M. D. Furnish, M. L. Elert, T. P. Russell, and C. T. White (AIP Conf. Proc. (2006)), p. 670.
12. J. F. Bingert, B. L. Henrie, and D. L. Worthington, Metall. Mater. Trans. A **38**, 1712 (2007).
13. F. Llorca and G. Roy, in *Proceedings of the 13th APS Topical Conference on Shock Compression of Condensed Matter, Portland, Oregon, United States, July 20–25, 2003*, Ed. by M. D. Furnish, Y. M. Gupta, and J. W. Forbes (AIP Conf. Proc. (2004)), p. 589.
14. W. R. Thissell, A. K. Zurek, D. L. Tonks, and R. S. Hixson, in *Proceedings of the Conference on Shock Compression of Condensed Matter, Snowbird, Utah, United States, June 28–July 2, 1999*, Ed. by M. L. Elert, W. T. Buttler, M. D. Furnish, W. W. Anderson, and W. G. Proud (AIP Conf. Proc. (2000)), p. 451.
15. L. C. Chhabildas, W. M. Trott, W. D. Reinhart, J. R. Cogar, and G. A. Mann, in *Proceedings of the Conference of the APS Topical Group on Shock Compression of Condensed Matter, Atlanta, Georgia, United States, June 24–29, 2001*, Ed. by M. D. Furnish, N. N. Thadhani, and Y. Horie (AIP Conf. Proc. (2002)), p. 483.
16. M. D. Furnish, G. T. Gray III, and J. F. Bingert, in *Proceedings of the 17th Biennial International Conference of the APS Topical Group on Shock Compression of Condensed Matter, Nashville, Tennessee, United States, June 28–July 3, 2009*, Ed. by M. L. Elert, W. T. Buttler, M. D. Furnish, W. W. Anderson, and W. G. Proud (AIP Conf. Proc. (2009)), p. 1089.
17. M. D. Furnish, W. D. Reinhart, W. M. Trott, L. C. Chhabildas, and T. J. Vogler, in *Proceedings of the 14th APS Topical Conference on Shock Compression of Condensed Matter, Baltimore, Maryland, United States, July 31–August 5, 2005*, Ed. by M. D. Furnish, M. L. Elert, T. P. Russell, and C. T. White (AIP Conf. Proc. (2006)), p. 615.
18. J. P. Cuq-Lelandias, M. Boustie, L. Soulard, L. Berthe, T. De Resseguier, P. Combis, J. Bontaz-Carion, and E. Lescoute, RPJ Web Conf. **10**, 00014 (2010).
19. D. B. Holtkamp, D. A. Clark, E. N. Ferm, R. A. Gallegos, D. Hammon, and W. F. Hamsing, in *Proceedings of the Conference of the APS Topical Group on Shock Compression of Condensed Matter, Portland, Oregon, United States, July 20–25, 2003*, Ed. by M. D. Furnish, N. N. Thadhani, and Y. Horie (AIP Conf. Proc. (2004)), p. 739.
20. J. R. Asay, T. Ao, T. J. Vogler, J.-P. Davis, and G. T. Gray III, J. Appl. Phys. **106**, 073515 (2009).
21. L. E. Murr, M. A. Meyers, C. S. Niou, Y. J. Chen, S. Parru, and C. Kennedy, Acta Mater. **45**, 1, 157 (1997).
22. J. M. McNaney, L. M. Hsung, N. R. Barton, and M. Kumar, in *Proceedings of the 17th Biennial International Conference of the APS Topical Group on Shock Compression of Condensed Matter, Nashville, Tennessee, United States, June 28–July 3, 2009*, Ed. by M. L. Elert, W. T. Buttler, M. D. Furnish, W. W. Anderson, and W. G. Proud (AIP Conf. Proc. (2009)), p. 1127.
23. G. I. Kanel', Prikl. Mekh. Tekh. Fiz. **42** (2), 194 (2001).
24. G. I. Kanel', S. V. Razorenov, A. V. Utkin, and V. E. Fortov, *Shock-Wave Phenomena in Condensed Matter* (Yanus-K, Moscow, 1996) [in Russian].
25. L. M. Barker and R. E. Hollenbach, J. Appl. Phys. **43**, 4669 (1972).
26. G. E. Duvall, in *Stress Waves in Anelastic Solids*, Ed. by H. Kolsky and W. Prager (Springer, Berlin, 1964), p. 20.
27. G. I. Kanel, S. V. Razorenov, A. V. Utkin, V. E. Fortov, K. Baumung, H. U. Karow, D. Rush, and V. Licht, J. Appl. Phys. **74** (12), 7162 (1993).
28. T. Antoun, L. Seaman, D. R. Curran, G. I. Kanel, S. V. Razorenov, and A. V. Utkin, *Spall Fracture* (Springer, New York, 2003).
29. A. V. Utkin, Prikl. Mekh. Tekh. Fiz. **38** (6), 157 (1997).
30. G. I. Kanel, Int. J. Fract. **163** (1–2), 173 (2010).
31. G. Roy, Thesis of Doctor of Sciences (University of Poitiers, Poitiers, France, 2003).

Translated by O. Borovik-Romanova